Strong Compression of a Magnetic Field with a Laser-Accelerated Foil

Hitoki Yoneda and Tomonori Namiki
Institute for Laser Science, University of Electro-Communications, Chofu, Tokyo 182-8585, Japan

Akinori Nishida and Ryosuke Kodama
Graduate School of Engineering, Osaka University, Suita,Osaka 565-0871, Japan

Youichi Sakawa, Yasuhiro Kuramitsu, Taichi Morita, Kento Nishio, and Takao Ide
Institute of Laser Engineering, Osaka University, Suita, Osaka 565-0871, Japan
(Received 27 March 2012; revised manuscript received 14 June 2012; published 21 September 2012)

We demonstrate the generation of high magnetic fields for condensed matter research using a high-power laser system. A cavity in which a seed magnetic field is applied is compressed by a kJ ns laser pulse. The time history of the compressed magnetic field is monitored by observing the Faraday effect rotation of polarization of a probe pulse in a glass fiber. To maintain a low-temperature condition in the final high-field region, we put a high-resistance foil around the final compression area. If we assume the length of the compression region is equal to the laser spot size, a magnetic field of more than 800 T is observed by Faraday rotation. Because of the large mass of the compression foil, this high magnetic field is sustained during almost 2 ns. During compression, a rarefaction wave from the backside of the accelerated foil and expanding material from the inner protection foil affect the magnetic field compression history, but the final compressed magnetic field strength agrees with the ratio between the initial sample area and the compressed cavity area.

DOI: 10.1103/PhysRevLett.109.125004 PACS numbers: 52.38.Mf, 07.55.Db

Matter in very strong magnetic fields is a promising research area [1]. Several methods have been proposed to generate magnetic fields larger than 1 MG. These include an electromagnetic field compression technique [2], a single-turn coil driven by a high current pulsed power machine [1,3], and liner implosions with chemical or electrical explosion [4,5]. There are also laser driving methods. The large temperature gradients near the laser focal spot generates large fields [6] as do hot electron currents driven by an ultraintense laser pulse [7], or a plasma jet induced by an ultrashort pulse laser [8]. Because of the higher current density in high-density plasma as compared to normal conductors, a larger magnetic field can be generated in or near to the dense plasma. However, to apply the generated magnetic field for condensed matter physics, a temperature below the melting point is required. Recently, a petawatt-level ultraintense laser has been used to generate a high current density in a high-density plasma. With this current, a magnetic field estimated at 75 000 T was reported [7]. Very recently, magnetic field compression by a laser-generated shock wave was proposed and a magnetic field of about 4000 T was observed [9]. But these methods are difficult to use for study of normal condensed matter because the temperature of the high magnetic field region is very high and the high magnetic field duration is short due to the pulse duration of the driving current or low mass of the compression piston.

At present, the electromagnetic flux compression method and single-turn generator have been used to investigate solid-state physics at magnetic fields up to several hundred tesla [1,10]. Using such strong magnetic fields, there have been studies of strong coupling between rotational-vibration energy and the cyclotron motion of electrons in the conduction band in semiconductors [7], for example. In such experiments, a large current is driven in a metal cylinder wall and the $J \times B$ force pinches this to compress the initial magnetic field applied inside the cylinder. The maximum compressed magnetic field strength is determined by the $J \times B$ force so that, to increase the compressed magnetic field, the main capacitor must be increased. That is a severe limitation for such experiments. To improve upon these techniques, we propose a method of achieving 1000 T magnetic fields by cavity compression using a laser-accelerated foil. According to the ablation pressure scaling, a pressure above 2.5 TPa is obtained at intensity of 1.2×10^{14} W/cm^2 and wavelength of 0.35 μm. This estimate implies that a 2500 T field could be achieved. For our proposed method of laser-accelerated piston impact, the maximum possible magnetic field is even larger than this as a result of the inertia of the piston. Even with the lower estimate, the field can apparently be larger than for the electromagnetic compression method. At magnetic field strengths larger than 2000 T, the free electron cyclotron energy is comparable to the electron excitation energy and the calculated Larmor radius is similar to the atomic separation in metals. Therefore, new electronic structure conditions can be produced.

Experimental setup.—A schematic drawing of this experiment is shown in Fig. 1. The compression target is divided into the compression area, the sample area, and the "dumper." We use one beam-bundle illumination geometry so that a massive dumper is needed as an anvil for the compression. The compression foil is typically a 20 μm thick titanium foil while the inner protection foil is a 10 μm NiCr foil. The material of the dumper is stainless steel. Typical dimensions of this target are: radius of the compression cavity is 0.3–0.7 mm; the radius of the sample area is about 150 μm. The dumper radius is 0.5 mm. The stainless steel dumper should have a thickness large compared to the skin depth determined by the compression duration while the protection foil (NiCr) should be thin compared to its skin depth. The compression foil (Ti) must be thicker than its skin depth. This thickness is also limited by consideration of hydrodynamic efficiency from a comparison of the laser energy and the target kinetic energy. In addition, the mass of the compression foil should be enough larger than the product of the mass ablation rate for the laser intensity and the pulse duration of the design of the experiment. Typical numbers of these foil thicknesses are 20 μm for the accelerated Ti foil and 10 μm for the protection NiCr foil, respectively.

To generate the seed magnetic field, we use a 1 Ω, 20 kA pulse power system which is triggered by a laser spark gap. We use a pulse from the second harmonic of a pulsed YAG laser which is electrically synchronized with the main compression laser pulse. The jitter of this pulse power firing is about 1 ns. A 10-turn coil is connected with the feed from this power supply. This coil has an approximately 1.5 mm inner hole diameter and 8 mm outer diameter. The compression target is located (on axis) just next to this coil and its outer diameter and length are 1 mm and 1.5 mm, respectively, so that we expect almost uniform seed magnetic field inside the compression cylinder. The strength of the seed magnetic field is about 20 T and it is observed separately with a magnetic pickup coil.

To measure the temporal history of magnetic compression, a fused silica optical fiber runs through the sample area. It has a 100 μm core and 110 μm cladding. We use the same second harmonic YAG laser pulse that triggers the pulse power machine to measure the polarization rotation inside the fiber. The polarization rotation is measured by a combination of Wollaston prism and streak camera. On the slit of this camera, we have two orthogonal polarization images of the fiber transmission light. The Verdet constant of the fused silica is 2.05×10^{-2} [min./Oe/cm] for this probe wavelength.

To check the two-dimensional shape of the accelerated foil and plasma expansion inside the compressed cavity, we also use the same probe laser as a backlight source for a shadowgraph. Three 1 ns gated images with different gate timing are obtained for this purpose.

The kJ 3ω light from a Gekko XII HIPER laser system of Osaka University is used for the compression experiment. The intensity on the target and its pulse duration are 10^{15} W/cm^2 and 0.5 ns, respectively. The focused diameter is 0.5 mm and matches the cross-sectional size of the compressed cavity.

Experimental results.—Fig. 2 shows a two-dimensional image of the compressed cavity at 1 ns after the peak of the main compression pulse. We indicate both the initial foil and protection foil position with dotted lines. This figure is

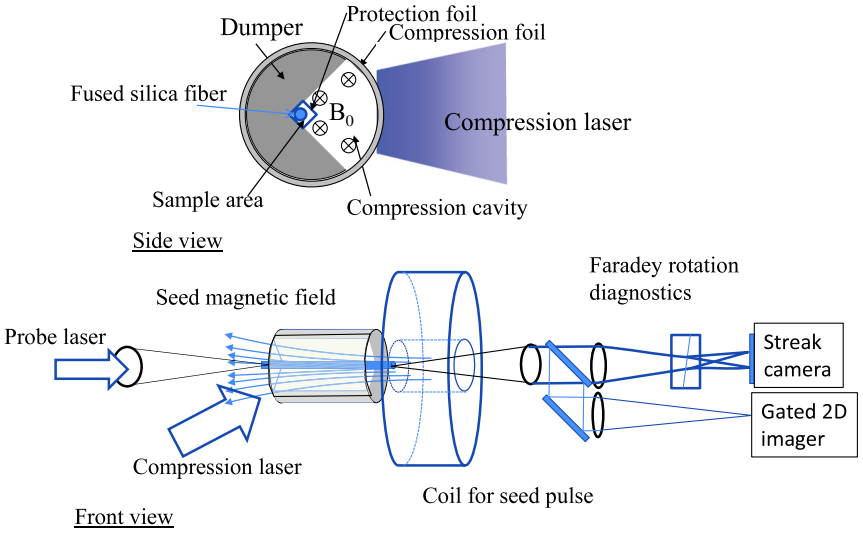

FIG. 1 (color online). A schematic drawing of the experiment. Side view (top) and front view (bottom). The compression target is divided into the compression cavity, the sample area, the compression foil, and the dumper. The compression foil is accelerated with the compression laser pulse. The seed magnetic field is prepared with a 1 Ω, 20 kA pulse power system. To measure the temporal history of magnetic compression, a fused silica optical fiber runs through the sample area. The polarization rotation is measured by a combination of polarizer and streak camera.

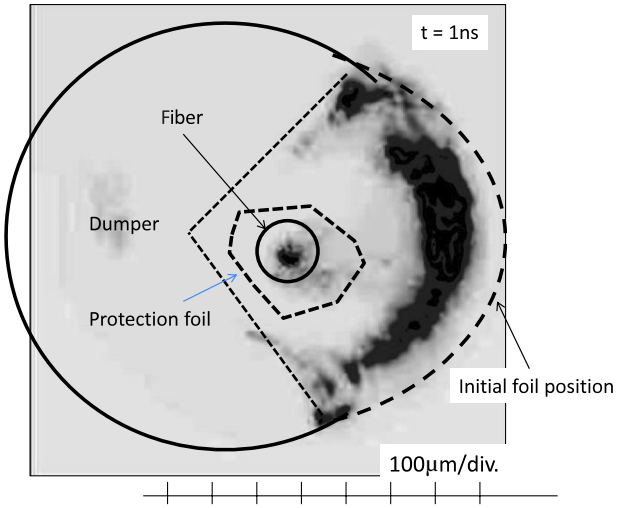

FIG. 2 (color online). Two-dimensional image of the compressed cavity at 1 ns after the peak of the main compression pulse. The black area means good transmission of the backlighting beams. The compression laser illuminates the compression foil from the right side. The compression foil uniformly moves inward.

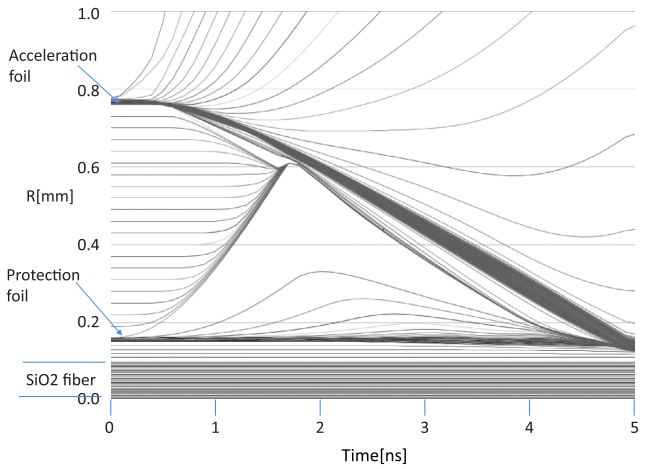

FIG. 3 (color online). Result of a one-dimensional hydrodynamic simulation for this target. We assume cylinder geometry and 10^{12} W/cm^2 additional laser flux (leakage) is applied to the protection foil surface. Even though the front of the expansion from the protection foil moves faster than the massive compression foil, this plasma can be compressed by the inward moving foil.

a negative image so that the black area means good transmission of the backlighting beams. The compression laser illuminates the compression foil from the right side. As shown in this figure, the compression foil moves inward uniformly. In addition, we can see a large expansion of the protection surface. The speed of expansion of the protection foil is 2 or 3 times higher than that of the inward motion of the compression foil. The outer surface of the protection foil expands due to ablation caused by radiation from the rear surface of the accelerated foil or leakage of light from the main compression laser pulse. With the help of a hydrodynamics code, we estimate that the temperature of the rear surface of the accelerated foil is tens of eV after the first shock wave crosses it, if the foil is illuminated at an intensity of 5×10^{14} W/cm^2. This temperature is enough to emit radiation and to heat the interior of the compressed cavity. In fact, without the protection foil, the fiber transmission disappears as a result of heating of the fiber by this radiation. With the protection foil, the fiber transmission continues through the experiment and this verifies the low-temperature in the high-field region.

Figure 3 shows the result of a one-dimensional hydrodynamic simulation for this target. We assume cylinder geometry and 10^{12} W/cm^2 additional laser flux (leakage) is applied to the protection foil surface. In this simulation result, we observe a similar plasma expansion inside the compression cavity. However, even though the front of the expansion from the protection foil moves faster than the massive compression foil, the density of the expansion plasma is less than 10^{-3} g/cc so that this plasma can be compressed by the inward moving foil. In the two-dimensional green laser shadowgraph, after collision of the two components, we cannot observe the interior but we consider the compression should continue. In this simulation, the thermal isolation effect of the protection foil is clarified. The peak temperature in the region between the acceleration foil and the protection foil is 500 eV at $t = 4$ ns while that between the sample and the protection foil is 0.5 eV.

Figure 4 shows the time history of polarization change though the fused silica fiber in the sample area. The input probe laser is linearly polarized with Glan laser prism and one axis (I_1) of the Wollaston prism is matched to the incident probe light polarization axis. Therefore, before compression, I_1 is maximum while I_2 (the other axis) is minimum. In Fig. 4, we plot the ratio $Y = (I_1 - I_2)/(I_1 + I_2)$ to understand the polarization change independent of the intensity change in the probe light. This ratio determines $\cos 2\theta = (Y + 1)/2 + \delta$, where θ is polarization rotation angle and is a linear function of magnetic field strength. Because of multimode properties of the fiber, a small percentage δ (less than 5%) of the transmitted light is depolarized. If we assume the length of the compressed cavity equals the spot size of the compression laser (0.5 mm), we can calculate the magnetic field strength change occurring in the compression. In addition, we also estimate the radius of the cavity required for this field enhancement. This Faraday rotation measurement is tested with the uncompressed magnetic field in the solenoid coil powered by the 20 kA current. The measured magnetic field almost matches the calculated value. In Fig. 4, the time history of the magnetic field and the estimated radius of the cavity are shown. In this compression experiment, the initial cavity radius is 400 μm. A strong increase of the

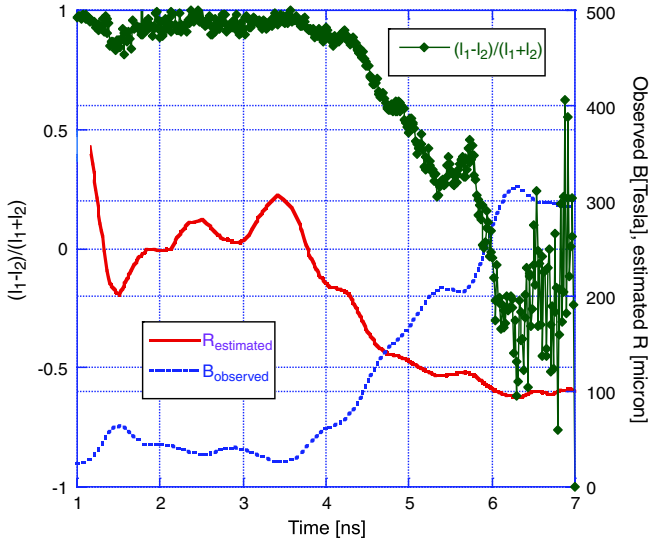

FIG. 4 (color online). Temporal history of polarization change though the fused silica fiber in the sample area. I_1 and I_2 are a pair of polarization component of the probe laser. We plot the ratio $Y = (I_1 - I_2)/(I_1 + I_2)$. The magnetic field strength change is calculated with assumption of 0.5 mm length of the compressed cavity. In addition, the radius of the cavity required for this field enhancement is estimated and plotted with these data.

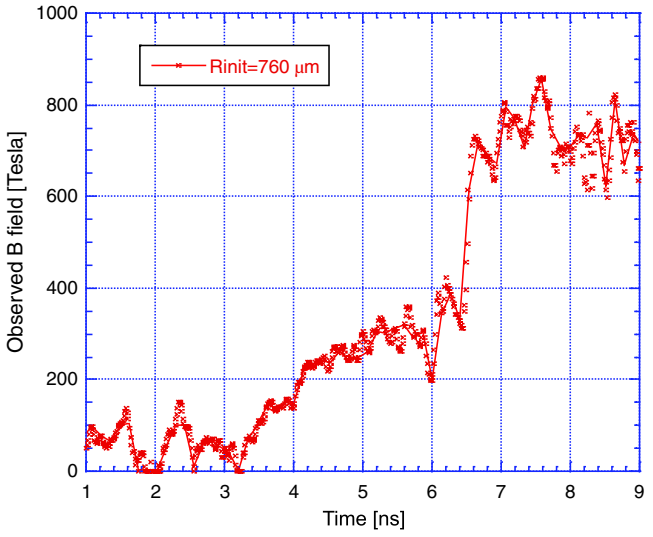

FIG. 5 (color online). Observed magnetic field for the larger cavity target. An 800 T magnetic field is observed. This is in reasonable agreement considering the seed field strength (20 T) and the compression ratio (6.9).

magnetic field is clearly observed. The speed of the cylindrical implosion at late time is about 200 μm/ns and this is similar to the prediction of the hydrodynamic simulation. In Fig. 4, it is found that the cavity size does not simply decrease. At early time, and again around $t = 5.5$ ns, a bouncing structure appears. If we compare the flow line in Fig. 3, the structure is caused by field redistribution due to the expansion plasma from the protection layer and an inward shock wave due to collision of the two plasma components. This idea is also supported by two-dimensional observation inside the cavity.(Fig. 2). The estimated conductivity of the plasma inside the cavity is 2×10^7 [S/m] when we use the plasma parameters ($Te = 500$ eV, $ne = 1 \times 10^{22}$ cm^{-3}) from the hydrodynamic simulation. The corresponding skin depth is less than 10 μm. Therefore, this expanded plasma inside the cavity has a large effect on the magnetic field compression. The maximum magnetic field strength is determined by the end of compression of the cavity at the wall of the sample area ($r \sim 100$ μm). In this design, the radius is compressed by a factor $\sim$4. The measured maximum magnetic field (20 T $\rightarrow$ $\sim$300 T) agrees with the square of this ratio. This means we successfully compress the cavity down to the design radius. During the compression, the light transmitted through the fiber decreases. That is caused by heating by scattering light or a heat wave penetrating the protection foil. In Fig. 4, even though there is large scatter of the polarization degree, the duration of the maximum field is about 1 ns. That duration is also an advantage for this method as compared to other laser-generated high magnetic field experiments.

To obtain a larger magnetic field strength, a larger cavity target was irradiated with similar intensity conditions. In Fig. 5, the observed magnetic field is shown for the larger cavity target which had initial radius of 760 μm. Because the radius of the sample area is the same as the previous case in Fig. 4, the maximum compression ratio in radius is expected to be 6.9. In the measurement of the Faraday rotation, we observe more than 800 T and this is in reasonable agreement considering the seed field strength (20 T) and the compression ratio. Consistent with the smaller cavity results, the maximum magnetic field is proportional to the areal compression ratio at least for our experimental conditions. The magnetic field pressure is still only about 1% of the compression pressure of the accelerated foil, so that we could compress more with a larger cavity size or smaller size of the sample area. We again see a nonsmooth field history but there are common features between small and large cavity cases. Evidently, shock wave and magnetic field penetration into the expansion plasma affect this temporal history.

Conclusion.—A high magnetic field generation by compression of a cavity with a laser-accelerated foil is proposed. We demonstrate the field compression and succeed in measuring the time history of the magnetic field during the compression. For the measurement, a key point is to protect the compression area from the thermal wave and radiation. This protection is also important for application of the high magnetic field to investigate condensed matter at fields in which even the electronic energy of atoms is strongly modulated by the electron cyclotron energy. Up to now, maximum magnetic field strength in this method is

more than 800 T. The maximum strength of the magnetic field is determined by the final compression radius caused by the massive wall of the sample area. The compression force is still sufficient to generate higher magnetic fields.

The authors thank Richard More for useful discussion of magnetic compression experiments. We also thank Ms. Y. Kimura for her technical support of making the targets. This research was partially supported by the Japanese Ministry of Education, Science, Sports, and Culture (MEXT), Grant-in-Aid, and by the joint research project of the Institute of Laser Engineering, Osaka University.

[1] F. Herlach and N. Miura, *High Magnetic Fields: Science and Technology*, Vol. 1 (World Scientific, Singapore, 2003).
[2] E. C. Cnare, J. Appl. Phys. **37**, 3812 (1966).
[3] C. H. Mielke and B. M. Novac, IEEE Trans. Plasma Sci. **38**, 1739 (2010); S Takeyama, H. Sawabe, and E. Kojima, J. Low Temp. Phys. **159**, 328 (2010).
[4] Yu. B. Kudasov *et al.*, J. Exp. Theor. Phys. **89**, 960 (1999).
[5] A. S. Dzurak *et al.*, J. Phys. B **246-247**, 40 (1998).
[6] J. A. Stamper, K. Papadooulos, R. N. Sudan, S. O. Dean, E. A. McLean, and J. M. Dawson, Phys. Rev. Lett. **26**, 1012 (1971).
[7] U. Wagner, M. Tatarakis, A. Gopal, F. N. Beg, E. L. Clark, A. E. Dangor, R. G. Evans, M. G. Haines, S. P. D. Mangles, P. A. Norreys, M.-S. Wei, M. Zepf, and K. Krushelnick, Phys. Rev. E **70**, 026401 (2004).
[8] S. Kahaly, S. Mondal, G. R. Kumar, S. Sengupta, A. Das, and P. K. Kaw, Phys. Plasmas **16**, 043114 (2009).
[9] J. P. Knauer, O. V. Gotchev, P. Y. Chang, D. D. Meyerhofer, O. Polomarov, R. Betti, J. A. Frenje, C. K. Li, M. J.-E. Manuel, R. D. Petrasso, J. R. Rygg, and F. H. Séguin, Phys. Plasmas **17**, 056318 (2010).
[10] N. Miura, H. Nojiri, P. Pfeffer, and W. Zawadzki, Phys. Rev. B **55**, 13598 (1997).